A direct measure of the frequency response of hot-wire anemometers: temporal resolution issues in wall-bounded turbulence

N. Hutchins · J. P. Monty · M. Hultmark · A. J. Smits

Abstract Based on the need to characterise the accuracy of hot-wire anemometry (HWA) in high Reynolds number wall-bounded turbulence, we here propose a novel direct method for testing the frequency response of various systems to very high frequency velocity fluctuations (up to 50 kHz). A fully developed turbulent pipe flow is exploited to provide the input velocity perturbations. Utilising the unique capabilities of the Princeton Superpipe, it is possible to explore a variety of turbulent pipe flows at matched Reynolds numbers, but with turbulent energy in different frequency ranges. Assuming Reynolds number similarity, any differences between the appropriately scaled energy spectra for these flows should be indicative of measurement error. Having established the accuracy of this testing procedure, the response of several anemometer and probe combinations is tested. While these tests do not provide a direct or definitive comparison between different anemometers (owing to non-optimal tuning in each case), they do provide useful examples of potential frequency responses that could be encountered in HWA experiments. These results are subsequently used to predict error arising from HWA response for measurements in wall-bounded turbulent flows. For current technology, based on the results obtained here, the frequency response of under- or over-damped HWA systems can only be considered approximately flat up to 5–7 kHz. For flows with substantial turbulent energy in frequencies above this range, errors in measured turbulence quantities due to temporal resolution are increasingly likely.

1 Introduction

There has been a concerted push over the last few decades towards higher Reynolds number facilities for studying wall-bounded turbulence, For example, the Princeton Superpipe (Morrison et al. 2004); the NDF at IIT Chicago (Hites 1997); the MTL at KTH Stockholm (Österlund 1999); the HRNBLWT at the University of Melbourne (Nickels et al. 2007); the LLF at DNW Netherlands (Fernholz et al. 1995); and the CICLoPE at Predappio (Talamelli et al. 2009). In general, these higher Reynolds number facilities will be characterised by smaller scales of turbulence and a higher-frequency content in the turbulence spectrum. Subsequently, this push to higher Reynolds numbers has reinvigorated attention to hot-wire sensor resolution. Building on the widely used results of Ligrani and Bradshaw (1987), there have been a slew of recent papers investigating spatial resolution of hot-wire sensors, with a particular emphasis on high Reynolds number wall-bounded turbulence (Hutchins et al. 2009; Chin et al. 2009, 2011; Smits et al. 2011; Örlü and Alfredsson 2010; Monkewitz et al. 2010; Segalini et al. 2011a, b). However, during this same period, the temporal resolution (or dynamic response) of the HWA system has received considerably less attention (see Ashok et al. (2012) for a recent attempt to consider both the effects of temporal and spatial resolution in grid generated turbulence).

There are two principal techniques that may be employed to determine the temporal response of a HWA system, both of which involve introducing some form of known perturbation into the system and measuring the response of the

N. Hutchins (✉) · J. P. Monty
Department of Mechanical Engineering, University of Melbourne, Parkville, VIC 3010, Australia
e-mail: nhu@unimelb.edu.au

M. Hultmark · A. J. Smits
Department of Mechanical and Aerospace Engineering, Princeton University, Princeton, NJ 08544, USA

anemometer's output signal. For *direct* methods, this perturbation is introduced as a velocity fluctuation into the flow in which the hot-wire probe is measuring. Such methods are attractively straightforward, unequivocally providing a direct measure of the system response to a velocity impulse (which is, after all, what we wish to know). However, the need to accurately impose high-frequency velocity perturbations on to a flow poses numerous experimental challenges (attempts at direct methods will be discussed below). In the absence of readily available convenient direct methods, the majority of users rely on *electronic* testing to estimate the system frequency response. The standard procedure involves injecting a square- or sine-wave perturbation into the bridge and observing the response of the anemometer's output signal. For most anemometers, there is typically some user-defined control of the square-wave response such that an 'optimum' response can be obtained (via adjustment of the bridge damping and inductance). The 'optimum' square-wave response is described by Freymuth (1977) as one in which there is a slight undershoot (of approximately 15 % of the maximum). Freymuth (1977) suggests that the cut-off frequency f_c of the system can be calculated from,

$$f_c = \frac{1}{1.3\tau_c} \tag{1}$$

where τ_c is the time from the start of the square-wave input to the point where the response has decayed to 3 % of its maximum value [see Bruun (1995), for a good description of this]. In applying Eq. (1), it is often overlooked that Freymuth (1977) defined this for the -3 dB cut-off. That is, based on the above equation, one would expect a 50 % attenuation in HWA measured energy at frequency f_c (and for the under-damped systems suggested as 'optimum', this 50 % attenuation would be accompanied by substantial over-representation of energy at lower frequencies). Bruun (1995) acknowledges this short-coming, recommending a sine-wave test for situations where a truly flat response is required [see Oxlade et al. (2012) for a recent application of this technique]. Nonetheless, Eq. (1), or some related form, is often used to estimate the system response, with the subsequently determined cut-off frequency f_c often cited to evidence a systems ability to resolve the particular flow under investigation. Though there are numerous theoretical studies suggesting that the square-wave test can provide a reliable indication of the true response of HWA systems to a velocity impulse (e.g. Freymuth 1977), there are also a few notable exceptions in the literature highlighting cases where electronic testing seems less reliable. Hutchins et al. (2009) and Valente and Vassilicos (2011) both seem to suggest that in certain situations the true temporal response of HWA systems can be substantially slower than that indicated from electronic testing [even when the

response appears to conform to optimally damped second order behaviour (Watmuff 1995)]. In a review of hot-wire anemometry, Comte-Bellot (1976) notes, when discussing the electronic testing of dynamic response, that 'direct checks using flow perturbations are worth making'.

There are some notable examples in the literature where direct methods have been attempted. Khoo et al. (1995) placed a hot-wire sensor in the cavity between two discs, one of which had radially machined recesses and could be rotated. This apparatus was capable of imposing known flow perturbations onto the sensor. From these experiments, it was concluded that their HWA system (Dantec 56C01) could faithfully respond up to the 1,600 Hz perturbations that this experimental apparatus was capable of producing. Ko and Ho (1977) used an audio speaker to superimpose a plane acoustic wave onto the flow through a pipe. This enabled them to test the response of a hot-wire sensor within the pipe flow at frequencies up to 8 kHz. From these experiments, they concluded that their system exhibited a flat response (to within ± 3 dB) for $0.14 < f < 8$ kHz. Perry and Morrison (1970) placed a hot-wire sensor in the periodic vortex street shed from a cylinder. Using this technique, they were able to test the dynamic response of their system at frequencies up to approximately 10 kHz. They found that their in-house system was flat up to approximately 8 kHz, while the tested Disa 55A01 anemometer exhibited a 3dB attenuation at 6 kHz. In this case, both directly measured responses were found to closely match those predicted from electronic square-wave testing. A further variant of direct testing is those experiments that have sought to test the frequency response of the HWA system by rapid cyclical heating of the hot-wire sensor element. As an early example, Kidron (1966) heated the sensor element (operated in constant current mode) using modulated microwaves. Bonnet and Roquefort (1980) used a modulated laser to heat the sensor (operated in constant temperature mode), finding good agreement with electrical sine-wave testing.

For this study, based on the need to investigate the accuracy of hot-wire anemometers in high Reynolds number turbulent boundary layers, we aim to pursue a direct method for testing the dynamic response of a HWA system to very high frequency velocity fluctuations (up to 50 kHz). To achieve this, we will use a turbulent wall-bounded flow itself to provide the input velocity perturbations.

2 Rationale

The assumption of Reynolds number similarity states that two fully developed turbulent pipe flows with differing characteristic velocity, lengthscale and kinematic viscosity, yet the same Reynolds number, must be identical in all

appropriately scaled statistics. We here exploit this assumption to vary the frequency content of the turbulent spectrum in order to investigate the frequency response of hot-wire anemometers.

Although the idea of this set of measurements is very simple, the execution is possible only because of the unique capabilities of the Princeton Superpipe (Zagarola and Smits 1998; Smits and Zagarola 2005). By pressurising the entire pipe flow facility up to 220 atm, the kinematic viscosity of the working fluid (air) can be altered by a factor of more than 100. This capability is primarily motivated by the desire to operate at very high Reynolds numbers (without experiencing compressibility effects); however, we here exploit this unique feature to test multiple turbulent pipe flows, all at matched Reynolds numbers, but with vastly differing centreline velocities (and thus vastly differing frequency content).

The most convenient Reynolds number for fully turbulent pipe flow is the friction Reynolds number or Kármán number, defined as,

$$Re_\tau = \frac{U_\tau R}{\nu} \tag{2}$$

where U_τ is the friction velocity, ν is kinematic viscosity and R is the pipe radius. For a given facility, the radius R is fixed, and Re_τ is typically altered by changing the centreline velocity (which will alter U_τ). In the case of the Superpipe, we also have the option of altering ν.

In the lower part of a turbulent boundary layer, we know that the smallest scales of turbulence have a size that can be expressed in terms of the viscous lengthscale ν/U_τ. We also know that (close to the wall) these smallest scales will convect at a speed that approximately scales on U_τ. Therefore, the small-scale turbulent energy will have a frequency observed by a stationary observer that will scale as,

$$f \propto \frac{U_\tau^2}{\nu} \tag{3}$$

In fact, Hutchins et al. (2009) have shown over a range of Reynolds numbers that the highest frequencies in a turbulent boundary layer are fixed at,

$$f_m \approx \frac{U_\tau^2}{3\nu}. \tag{4}$$

Comparing Eqs. (2) and (3), we note that Reynolds number scales on U_τ/ν, while the maximum frequency in the flow scales on U_τ^2/ν. Consider two experiments conducted in the Superpipe: experiment 1 is performed at a given centreline velocity U_0 and ν. For experiment 2, if we now halve the friction velocity U_τ (by halving the centreline velocity) and halve the kinematic viscosity ν (by increasing the pressure), the Reynolds number will remain the same, but the frequency content of the flow will be reduced by a factor of 2 (f will be halved according to Eq. 3). In other words, the viscous lengthscale (the ratio ν/U_τ) remains unaltered between experiments 1 and 2, but the viscous timescale has been altered. Consider a hot-wire probe, inserted into a fully developed turbulent pipe flow at a fixed distance z from the wall for both experiments. The single-normal hot-wire probe has a sensor length l and diameter d. In terms of key experimental parameters, the viscous scaled wall-normal position z^+ ($=zU_\tau/\nu$) for the fixed probe will not change between experiments with matched Re_τ. In addition, the viscous scaled sensor length l^+ will also remain constant, and thus, there will be no variation in the spatial resolution of the probe (Ligrani and Bradshaw 1987; Hutchins et al. 2009). Thus, all experimental conditions will remain unchanged other than the frequency content of the turbulence. Based on the assumption of Reynolds number similarity, any differences between the spectral content of the two measured signals can therefore only be attributed to the frequency response of the anemometry system. This simple idea forms the basis of the measurements performed here.

This idea also implicitly relies on the notion that the heat transfer from the wire is primarily a function only of Reynolds number. The equation for the heat transfer from the wire, and thus the voltage output from the anemometer, is strictly a function of Reynolds number and Prandtl number (Bruun 1995; Li et al. 2004). However, since in this case the Reynolds number is held constant, and since the Prandtl number is only a very weak function of pressure (Li et al. 2004), one might expect the mean output voltage from the anemometer to be relatively invariant across the five experiments described above. This assumption is important, since the stability of the system is directly related to the mean cooling of the wire. For the experiments listed below

Table 1 Experimental parameters for the five matched cases with CTA1

e	Pressure (kPa)	$\nu\,(\times10^6)\,(\mathrm{m^2 s^{-1}})$	$U_0(\mathrm{ms^{-1}})$	$U_\tau(\mathrm{ms^{-1}})$	Re_τ	z (mm)	z^+	l (mm)	l^+	Probe	$f^+ = 0.01$ (kHz)
1	249	6.24	27.0	1.00	10,385	0.5	80.3	0.5	80.3	55P15	1.61
2	329	4.73	20.5	0.76	10,391	0.5	80.3	0.5	80.3	55P15	1.22
3	459	3.39	14.7	0.55	10,395	0.5	80.4	0.5	80.4	55P15	0.88
4	758	2.05	8.9	0.33	10,401	0.5	80.4	0.5	80.4	55P15	0.53
5	2,156	0.72	3.1	0.12	10,383	0.5	80.3	0.5	80.3	55P15	0.19

(experiments $e1$–$e5$ in Table 1, which range from a pressurisation of 2.5 atm up to 22 atm), the variation in mean output voltage is <1 SD of the fluctuating voltage measured at $z^+ = 80$. This variation in mean voltage (and hence heat transfer) is equivalent to a change in mean velocity of ≈ 7 % of the centreline velocity U_0, indicating that the effective cooling or heat transfer from the sensor, and thus the stability of the system, is almost invariant for these constant Reynolds number experiments (Appendix 1 indicates that such small changes in mean heat transfer are unlikely to substantially alter the stability of the system).

3 Experiments

3.1 Anemometry and probes

In total, three different anemometers were tested. These are referred to throughout as CTA1, CTA2 and CTA3. We make no claims here to have explored the entire performance space for each anemometer, nor do we claim that the systems tested are optimally damped or optimally configured. The reported behaviour will be specific to the particular configurations selected here, and as such, a different user may attain different performance. For these reasons, we have chosen not to name the anemometer systems. The purpose of these experiments is to provide a test of the direct response of the system to velocity perturbations, which may then serve as a comparison with the more widely applied standard electronic test.

Two probe types were investigated. For the majority of measurements, a slightly modified Dantec 55P15 boundary-type probe was used, with prong spacing 1.5 mm. Wollaston wires are soldered to the prong tips and etched to produce a 2.5-µm-diameter platinum-sensing element of length 0.5 mm. The un-etched portion (or stubs), which are 0.5 mm in length, have an estimated diameter of 40 µm. These probes are operated with an overheat ratio of 1.8 yielding a mean wire temperature of approximately 240 °C. The in-house Princeton nanoscale thermal anemometry probe (NSTAP) was also tested, with a platinum sensor of length 60 µm (see Kunkel et al. 2006; Bailey et al. 2010; Vallikivi et al. 2011, for full details). The NSTAP was operated with an overheat ratio of 1.3 yielding a mean wire temperature of approximately 210 °C.

3.2 Experimental conditions

Based on the notion that Re_τ would be held constant, we also know that the ratio,

$$S = \frac{U_0}{U_\tau},$$ (5)

would remain unchanged. The first step in these measurements was to approximately determine the value S for the Reynolds number at which we would be conducting experiments. The static pressure drop was measured in the initial unpressurised case to determine skin friction, yielding a value of $S = 27$ for $Re_\tau \approx 10{,}000$.[1] The Superpipe was pressurised from approximately 2.5 atm up to approximately 22 atm over a typical series of five experiments. For each pressure, the centreline velocity is carefully adjusted such that the ratio U_0/ν (and thus the viscous lengthscale ν/U_τ) is held constant. Table 1 shows experimental conditions for the test of CTA1. The table is loosely divided into sections. The first group of parameters demonstrates that by careful adjustment of the Superpipe pressurisation and the centreline velocity, the same Re_τ can be attained for a range of centreline velocities ranging from 3 to 27 ms^{-1}. The variation in Re_τ is <0.3 %. The second group of parameters reassures that key experimental parameters z^+ (the wall-normal position of the probe) and l^+ are virtually unaltered. The final column shows the frequency associated with $f^+ = 0.01$, which is the approximate non-dimensional frequency corresponding to the near-wall turbulent energetic peak due to the near-wall cycle (see for example Hutchins et al. 2009). It is clear that this set of matched experiments will have different frequency content in the turbulent spectra (the frequency content is shifted by almost an order of magnitude).

Hot-wire signals for all experiments were sampled at 300kHz using a Data Translation DT9832 16-bit analogue-to-digital converter (ADC). The ADC has an input range of ±10 V, giving a bit resolution of ≈0.3 mV (the standard deviation of the sampled output from the anemometer is approximately 1 V). Hutchins et al. (2009) estimate that energy in turbulent boundary layers is negligible for $t^+ < 3$. The sampling rate of 300 kHz corresponds to $\Delta t^+ \approx 0.07$–0.5 for these experiments. Since the sampling frequency sufficiently exceeds the maximum frequency content of the turbulent energy, the Nyquist criterion is met. Hence, aliasing will not be an issue and analogue filters are not employed. To guarantee equivalent convergence in energy spectra, the sample length T was nominally fixed at 37,000 boundary layer turnover times ($TU_0/r = 37{,}000$). Thus, T increased from 120 s for experiment 1 to approximately 1,000 s for experiment 5.

The particular set of experiments detailed in Table 1 was conducted with the probe at approximately 80 wall units

---

[1] It should be noted that the precise value of S is not crucial to these experiments. An estimate is good enough. Any error in S will only slightly alter the overall Reynolds number at which we conducted the experiments (along with the z^+ and l^+ values). More importantly, the estimate of S in no way influences how well matched the experiments are in terms of Re_τ, z^+, l^+, etc.
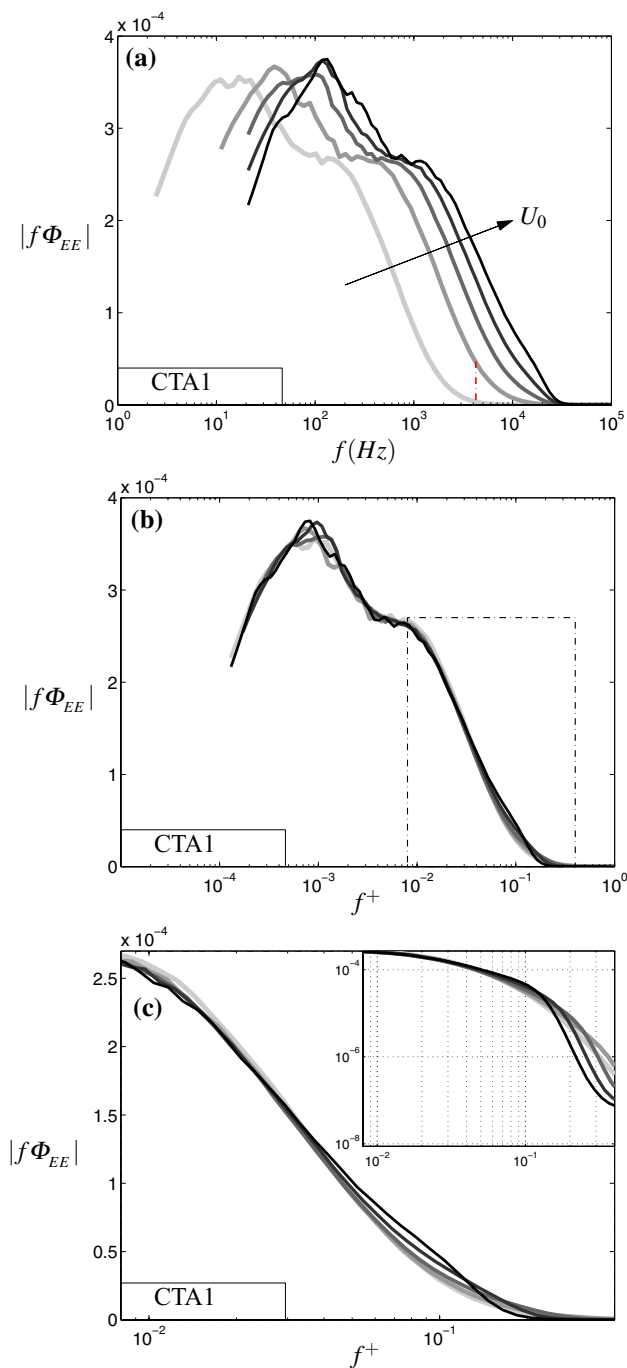
Fig. 1 Pre-multiplied energy spectra from the CTA1 experiment described in Table 1 shown for **a** dimensional frequency in Hz, the *dot-dashed vertical line* represents $f_l = 1/t_l$ for case $e5$, **b** non-dimensional frequency f^+, **c** zoomed view of the region bounded by the *dashed rectangle* in plot **b**. The *inset* in plot **c** shows the same zoomed view with a logarithmic ordinate. *Line shading* indicates centreline velocity from *light* (lowest U_0, $e = 5$) to *dark* (highest U_0, $e = 1$)

from the wall. For later experiments, the probe was moved closer to the wall. Figure 1 shows the pre-multiplied energy spectra ($f\Phi_{EE}$, where Φ_{EE} is the energy spectrum of

the voltage fluctuations) for the five experiments. Note that these spectra are based on uncalibrated voltage signals. There are some noise spikes present in the raw spectra at consistent frequencies for all anemometers (due to noise sources in the lab). Spectra are smoothed and interpolated at these frequencies to remove these spikes. The pre-multiplied spectra are normalised such that the area under the low-frequency portion of the curve ($1{,}000 < t^+ < 4{,}000$) is forced to 1 for all experiments. The notation of vertical parentheses is used to denote normalised spectra (i.e. $|f\Phi_{EE}|$). This normalisation bypasses the need for probe calibration, thus avoiding all experimental uncertainty introduced by hot-wire drift. Perry and Li (1990) have demonstrated that uncalibrated voltage signals can give an accurate representation of the true velocity spectra. Measurement error aside, Reynolds number similarity insists that all appropriately scaled spectra should be identical. The only additional assumption relied on here is that the large-scale measured energy (the low-frequency content) will be immune to the temporal resolution issues of the anemometer.

4 Results

4.1 CTA1

All data presented here are for the standard probe tip (55P15) at $z^+ \approx 80$. Figure 1a shows pre-multiplied energy spectra as a function of frequency for the experiments described in Table 1, demonstrating that this set of matched experiments has a widely varying frequency content. The darkest line, representing experiment 1 with the highest U_0 (and lowest pressure), has turbulent fluctuations at much higher frequencies than the other experiments (shown by the lighter shaded lines). The lowest speed experiment (experiment 5, the lightest line) will have the lowest frequency content and thus will be the most immune to temporal resolution issues. For the purposes of this experiment, we must consider this curve as the baseline (the most 'correct' measurement), against which the other experiments are compared.

Figure 1b shows the same spectra normalised by the viscous timescale (same data, with f^+ on the x axis). Non-dimensionalised in this way, the spectra seem to collapse quite well (there is of course the usual convergence issues at the low-frequency end). Indeed, if temporal resolution were not a problem for the anemometer, Reynolds number similarity would suggest that all spectra should be identical. In spite of the apparent collapse in Fig. 1b, a closer inspection of the higher-frequency end of the spectra does show some systematic differences. Figure 1c shows a zoomed view of the area bounded by the dashed rectangle in

Fig. 1b. In this zoomed view, we see systematic departures between the spectra. There is a very pronounced region centred around $f^+ = 0.08$ for which the higher speed flows (darker lines) record more energy than the baseline (lightest curve). There are signs that at higher f^+ this trend might reverse. There is also a less pronounced, but systematic trend centred around $f^+ = 0.015$, where the higher speed flows register reduced energy as compared to experiment 5. We know that any differences between the baseline case (experiment 5) and the other experiments must be due to temporal resolution issues. For each experiment number e, and at each value of f^+, we can define a difference function χ, as the fractional variation of the pre-multiplied spectra for a given experiment e (where $e = 1, 2, 3$ or 4) about the baseline case (experiment 5),

$$\chi_e(f^+) = \frac{|f\phi_{\mathrm{EE}}(f^+)|_e - |f\phi_{\mathrm{EE}}(f^+)|_5}{|f\phi_{\mathrm{EE}}(f^+)|_5} \quad (6)$$

So for a given experiment e, the function χ_e is a measure of the missing measured energy at each non-dimensional frequency f^+. A nonzero result for χ_e indicates that the anemometer is not accurately resolving energy at the higher frequency f_e where

$$f_e = \frac{f^+ U_{\tau_e}^2}{\nu_e}$$

Thus, if we plot χ_e versus f_e, we should obtain a measure of the attenuation due to the anemometer as a function of frequency. This is effectively a transfer function, with the input signal being the turbulent fluctuations measured in experiment 5 (the most accurate data in terms of temporal resolution) and the output signal the turbulent fluctuations measured in a higher-frequency experiment e. This result is shown in Fig. 2 for experiments 1–4. The difference function χ_e is evaluated across the energetic range of turbulence for $e = 1 \rightarrow 4$ within the range $t_l^+ < t^+ < 3{,}000$, where $1/t_l^+$ is the frequency at which the energy from the trusted signal $e5$ falls below 1 % of the maximum energy [t_l^+ equals 3–4 for the range of experiments shown here (see Fig. 1a)]. It is clear from Fig. 2 that the attenuation (and amplification) due to the temporal response of the anemometer system is relatively consistent across all experiments, providing confidence in the robustness of this technique. As further validation, it is also noted that the same curve for χ_e can be obtained by using experiment $e4$ as the baseline (provided any attenuation inherent in the baseline is iteratively corrected for).

The curves shown for χ_e in Fig. 2 are relatively noisy within the range $10 < f_e < 300$ due to the general lack of convergence in the low-frequency end of the spectra (as shown in Fig. 1a), yet seem to collapse quite well for higher frequencies. Beginning at $f_e \gtrsim 500\,\mathrm{Hz}$, there is a clear
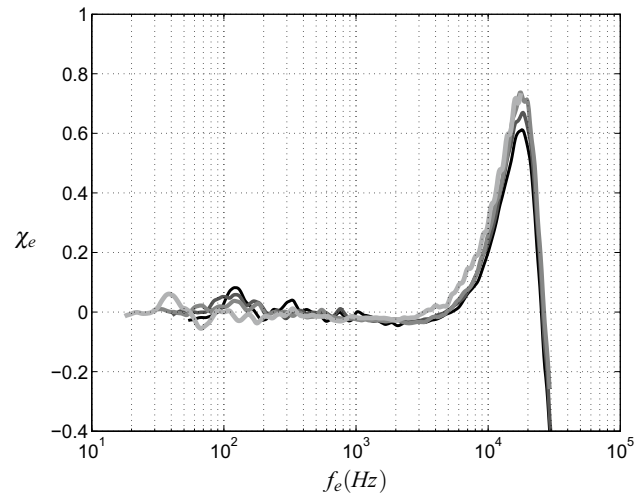

Fig. 2 The spectral difference parameter χ_e calculated for experiments $e = 1, 2, 3$ and 4. *Line shading* indicates centreline velocity from *light* (lowest U_0) to *dark* (highest U_0)

attenuation in the spectra measured by the anemometer. This attenuation peaks at approximately 4 % ($\chi_e = -.04$) in the range $1{,}000 < f_e < 3{,}000$. The onset of this attenuation is presumably related to the thermal inertia of the sensing element. Beyond this, at higher frequencies, we note that this trend reverses, and there is an increasing over-representation of energy beginning at frequencies in excess of $f_e \approx 5{,}000\,\mathrm{Hz}$ and peaking at $f_e \approx 18{,}000\,\mathrm{Hz}$. At this peak frequency, the anemometer records energy that is approximately 60–70 % greater than the baseline. These results would seem to indicate that quite serious systematic errors may be present in hot-wire measured data due to temporal resolution issues, in situations where the flow contains substantial energy at frequencies $\gtrsim 5$ kHz.

To reassure that the effect demonstrated by Fig. 2 is really a product of the anemometer frequency response and not merely an artefact of experimental technique, a further test of CTA1 was conducted in which we deliberately over-damped the square-wave response. Figure 3 shows a comparison of these two cases: the initial case (which was under-damped, as shown in the top plots) and the new case (which was over-damped, shown in the lower plots of Fig. 3). Both the transfer function χ_e (plots a, c) and the associated measured square-wave response (plots b, d) are shown for both damping scenarios.[2] A comparison of plots (a) and (c) demonstrates that the degree of damping does

---

[2] The square-wave response is measured in situ, with the probe at the centreline of the pipe with the centreline velocity U_0 matched to the measured mean at $z^+ = 79$ for experiment $e5$. Since the pipe has a turbulent core, the measured square-wave response is extracted from the turbulent signal using a triggered/conditional averaging technique—see Appendix 2.
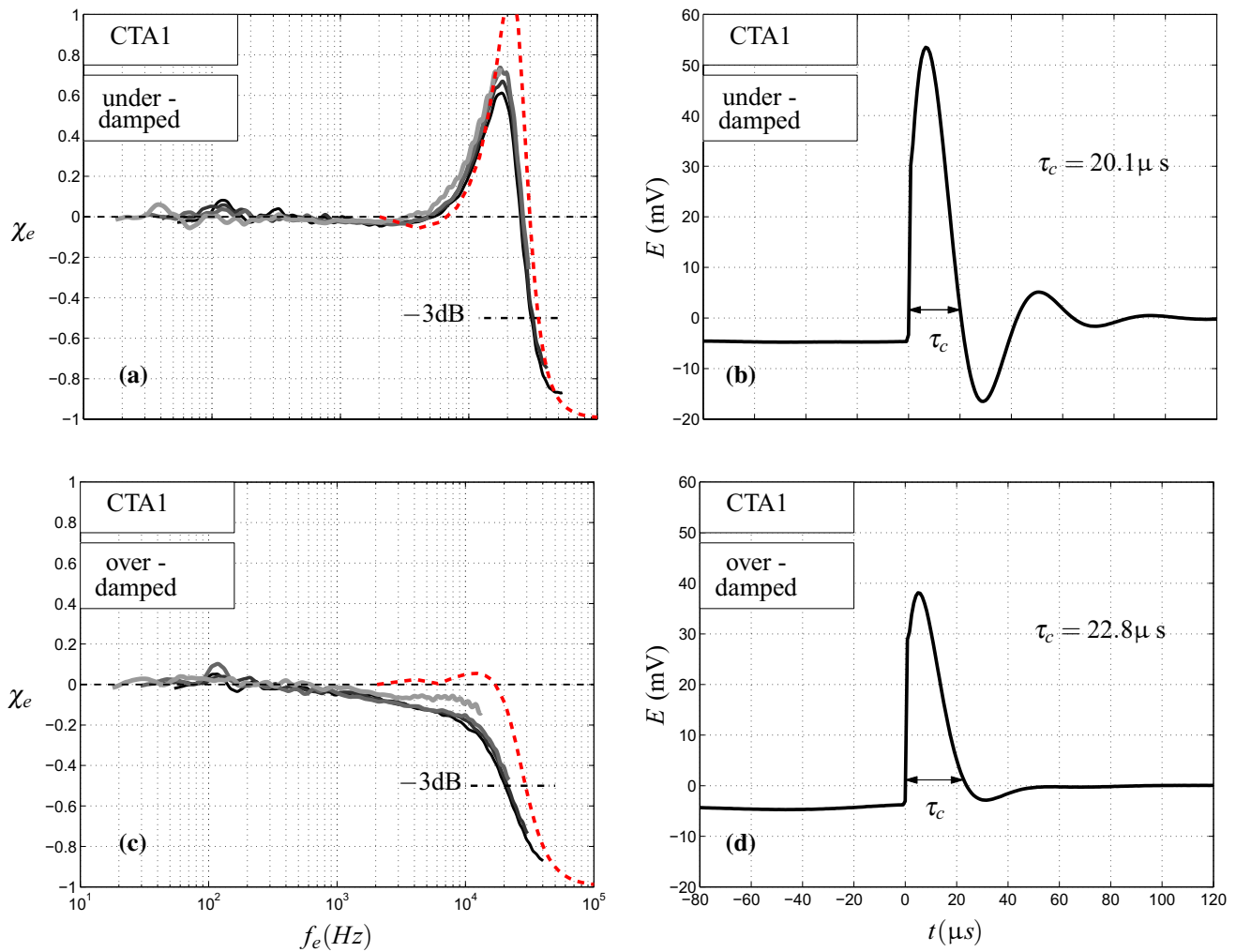
Fig. 3 Difference function (**a**, **c**) and the corresponding square-wave output (**b**, **d**) for (*top plots*) the under-damped CTA1 and (*bottom plots*) the over-damped CTA1. The *red dashed lines* in plots **a**, **c** show the normalised Fourier transform of the square-wave output. *Line shading* indicates centreline velocity from *light* (lowest U_0) to *dark* (highest U_0)

Table 2 Experimental parameters for the five matched cases of CTA2

e	Pressure (kPa)	$\nu\,(\times 10^6)\,(\mathrm{m^2\,s^{-1}})$	$U_0(\mathrm{ms^{-1}})$	$U_\tau(\mathrm{ms^{-1}})$	Re_τ	z (mm)	z^+	l (mm)	l^+	Probe	$f^+ = 0.01$ (kHz)
0	251	6.19	27.0	1.00	10,470	0.5	80.9	0.5	80.9	55P15	1.62
1	328	4.74	20.7	0.77	10,470	0.5	80.9	0.5	80.9	55P15	1.24
2	457	3.40	14.8	0.55	10,460	0.5	80.8	0.5	80.8	55P15	0.89
3	759	2.05	8.9	0.33	10,440	0.5	80.7	0.5	80.7	55P15	0.54
4	2,166	0.72	3.1	0.12	10,440	0.5	80.7	0.5	80.7	55P15	0.19

affect the behaviour of χ_e, with the over-damped case exhibiting none of the resonant behaviour evident for the under-damped case. Therefore, we are confident that this experimental technique and the parameter χ_e really are providing a measure of attenuation due to the temporal resolution of the anemometer system. The red dashed curves on Fig. 3a, c show the normalised energy spectra of the

response of the bridge to a step input in voltage (calculated from the FFT of the square-wave response shown in plots b and d). From classical control theory, the transfer function (the Bode plot) of a linear system is obtained by taking the Fourier transform of the impulse response of a system (the impulse response can be obtained by differentiating the square-wave responses shown in Fig. 3b, d). However,

Freymuth (1967) and Weiss et al. (2001) both suggest that the response of the *bridge* to a square-wave voltage input best indicates the *system* response to an impulse of velocity (where we define the system as the bridge plus the sensor). In the case of Fig. 3, the normalised energy spectra of the square-wave response yield a transfer function that approximately represents the experimentally observed behaviour (though, it should be noted that the energy spectra from the square-wave response overpredict the resonant peak in Fig. 3a). Though this can only be considered an observation (based on the nonlinearities of the system), the similarity is worth noting and is potentially useful. Regardless, the main purpose of Fig. 3 is to demonstrate that the experimentally determined transfer function χ_e is a measure of the response of the system, clearly capturing the underdamped and over-damped characteristics (shown on the top and bottom plots respectively of Fig. 3). It should be noted that neither response could be considered optimal. According to Bruun (1995), optimal responses are obtained when the overshoot is approximately 15 % relative to the maximum of the square-wave response. For the square-wave responses shown in Fig. 3c, d, the overshoots are approximately 30 and 8 % respectively for the under- and over-damped cases. Tests of CTA2 and CTA3 are also non-optimal configurations, where both systems are configured with large overshoots on the square-wave response, which would be expected to lead to under-damped behaviour.

One surprising aspect highlighted in Fig. 3 is that relatively minor changes in the square-wave response can indicate a shift from under- to over-damped behaviour. This is of particular importance for measurements with a large range of mean velocities (such as boundary layer flows) where the response can potentially vary quite significantly between the freestream (where the mean velocity is maximum) and close to the surface (where the velocity tends to zero). This is investigated in Appendix 1.

4.2 CTA2

Table 2 shows the conditions for a similar set of experiments designed to probe the frequency response of CTA2. Figure 4 shows the normalised spectra plotted against (a) dimensional and (b) non-dimensional frequency. Figure 4c shows an enlarged view of the region enclosed by the dot-dashed rectangle in plot (b). In Fig. 4a, there is a very clear modification in the shape of the high-frequency end of the spectra, centred around $10 < f < 30$ kHz. This manifests as an imperfect collapse of the non-dimensional spectra in plots b and c. In the same manner as for CTA1, the difference parameter χ_e is calculated and plotted in Fig. 5a. Again the parameter χ_e is noted to collapse
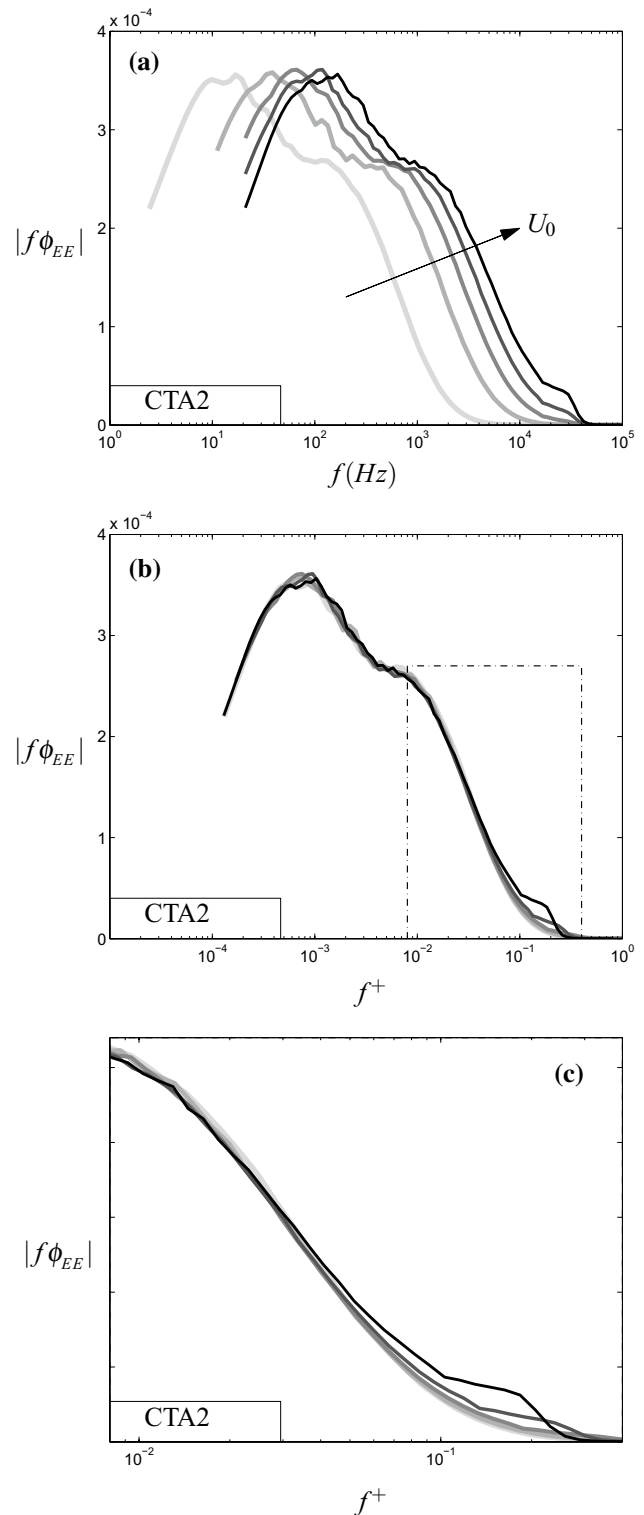

Fig. 4 Pre-multiplied energy spectra from the CTA2 experiment described in Table 2 shown for **a** dimensional frequency in Hz, **b** non-dimensional frequency f^+, **c** zoomed view of the region bounded by the *dot-dashed rectangle* in plot **b**. *Line shading* indicates centreline velocity from *light* (lowest U_0, $e = 5$) to *dark* (highest U_0, $e = 1$)

rather well across experiments $e = 1$–4. The behaviour is qualitatively similar to CTA1. There is a region of slight attenuation in the range $0.5 < f_e < 5$ kHz, peaking with 4–5 % attenuation in the range $1 < f_e < 3$ kHz. Beyond $f_e \approx 5$ kHz, there is a region of very pronounced amplification of the energy peaking at $f_e \approx 31$ kHz with

Fig. 5 The difference function (**a**) and the corresponding square-wave response (**b**) for the under-damped CTA2. The *red dashed line* in plot **a** shows the normalised Fourier transform of the square-wave output. *Line shading* on plot **a** indicates centreline velocity from *light* (lowest U_0) to *dark* (highest U_0)

a gain of approximately 5 (amplification of approximately 400 %). This amplification is much greater than for CTA1. It should be noted that CTA2 had been modified to enable compatibility with the NSTAP probe (see Sect. 4.4). As a consequence of this modification, some of the settings were disabled, which limited our ability to fine-tune the square-wave response. Nonetheless, this experiment serves as a useful indication of the direct response of an anemometer tuned in this manner. Again, the transfer function χ_e can be compared to the square-wave response that was used to tune the anemometer, as shown in Fig. 5b. The measured square-wave response clearly exhibits under-damped ringing behaviour which is reflected in the measured χ_e result. The normalised energy spectrum of the square-wave response is shown by the red dashed line in Fig. 5a. In this case, the 'Bode' plot again approximates the experimentally determined transfer function. The behaviour is qualitatively similar, but the square-wave response would indicate a peak amplification of $\approx 1{,}000$ % occurring at $f_e \approx 28$ kHz while the experimentally determined result χ_e indicates a peak amplification of 400 % at $f_e \approx 31$ kHz. Based on the approximate rule given by Freymuth (1977) and reproduced here as Eq. (1), one can compute the -3 dB drop-off for the square-wave test from the time τ_c (≈ 12 μ s), giving $f_c \approx 64$ kHz (although the rule is based on an optimal response, which is certainly not the case for this test). The experimentally determined χ_e would indicate a -3 dB drop-off in amplitude (energy gain of 0.5 or $\chi_e = -0.5$) at a slightly lower frequency of ≈ 57 kHz. The important point to notice from the experimentally determined transfer function χ_e is that the -3 dB drop-off is not an appropriate measure for accurate measurements in wall-bounded flow because,

1. The -3 dB drop-off is a 50 % reduction in energy. Freymuth (1977) recognises this point, suggesting that a "5 % drop might be more realistic for accurate measurements", where $f_{5\%} = 1/4\tau_c$.

2. For under-damped systems, there is a resonant peak leading to substantial over-representation of energy starting at frequencies that are approximately an order of magnitude lower than the -3 dB cut-off.
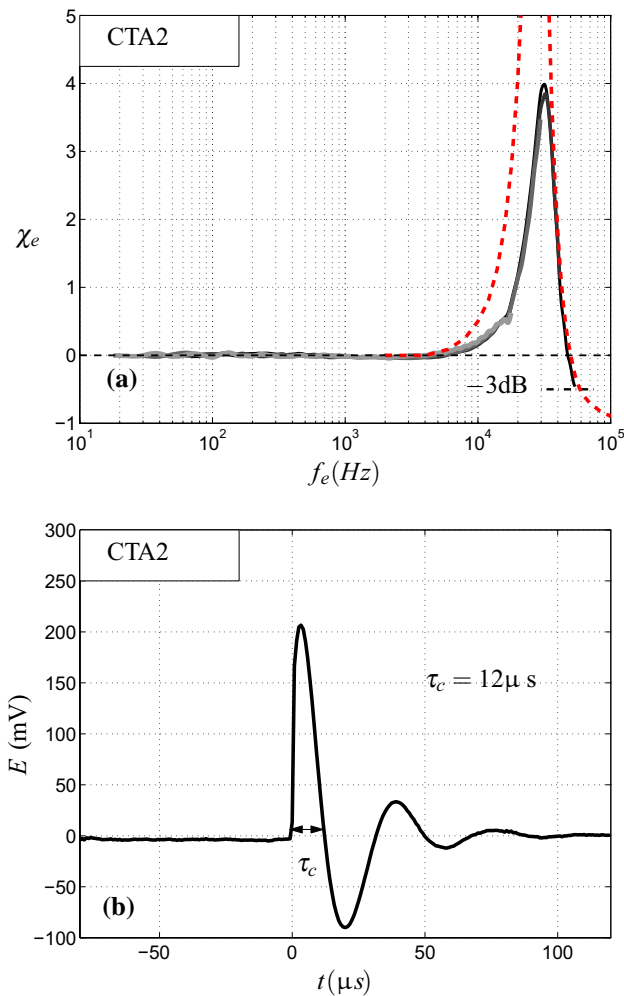
Table 3 Experimental parameters for the five matched cases for CTA3

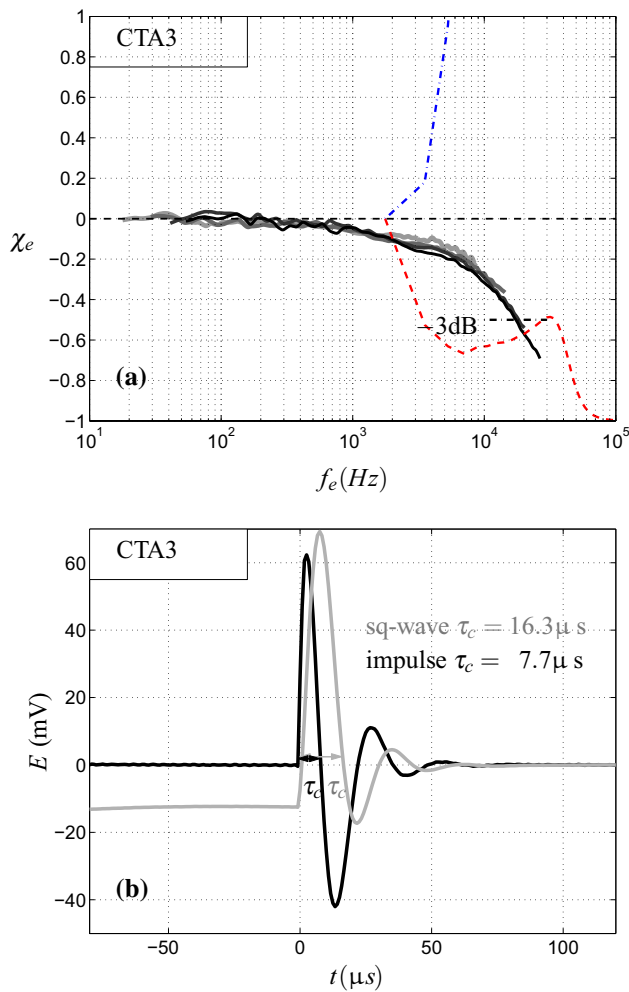| e	Pressure (kPa)	$\nu\,(\times 10^6)\,(\mathrm{m^2\,s^{-1}})$	$U_0(\mathrm{ms^{-1}})$	$U_\tau(\mathrm{ms^{-1}})$	Re_τ	z (mm)	z^+	l (mm)	l^+	Probe	$f^+ = 0.01\,(\mathrm{kHz})$
1	250	6.18	26.8	0.99	10,380	0.18	28.9	0.5	80.3	55P15	1.59
2	331	4.68	20.3	0.75	10,400	0.18	28.9	0.5	80.4	55P15	1.21
3	461	3.36	14.5	0.54	10,360	0.18	28.8	0.5	80.1	55P15	0.86
4	760	2.04	8.8	0.33	10,360	0.18	28.8	0.5	80.1	55P15	0.52
5	2,165	0.72	3.1	0.11	10,320	0.18	28.7	0.5	79.8	55P15	0.18

Fig. 6 **a** The difference function χ_e for CTA3 at $z^+ \approx 29$. *Line shading* indicates centreline velocity from *light* (lowest U_0, $e = 5$) to *dark* (highest U_0, $e = 1$). The *blue dot-dashed line* shows the normalised Fourier transform of the impulse test output. The *red dashed curve* shows the normalised Fourier transform of the integrated impulse response. **b** Corresponding (*black line*) impulse response (*grey line*) integrated impulse response

4.3 CTA3

Table 3 lists experimental parameters for a test of CTA3. The tests were conducted in the same manner as for CTA1 and CTA2, the only difference being that these experiments were conducted at a position closer to the pipe surface, with the wire positioned at $z = 0.18$ mm ($z^+ \approx 29$). Time constraints did not permit measurements at matched z^+; however, careful comparison of CTA1 and CTA2 at two different wall-normal positions has confirmed that the experimentally determined transfer function χ_e is relatively insensitive to changes in z^+. Figure 6a shows the
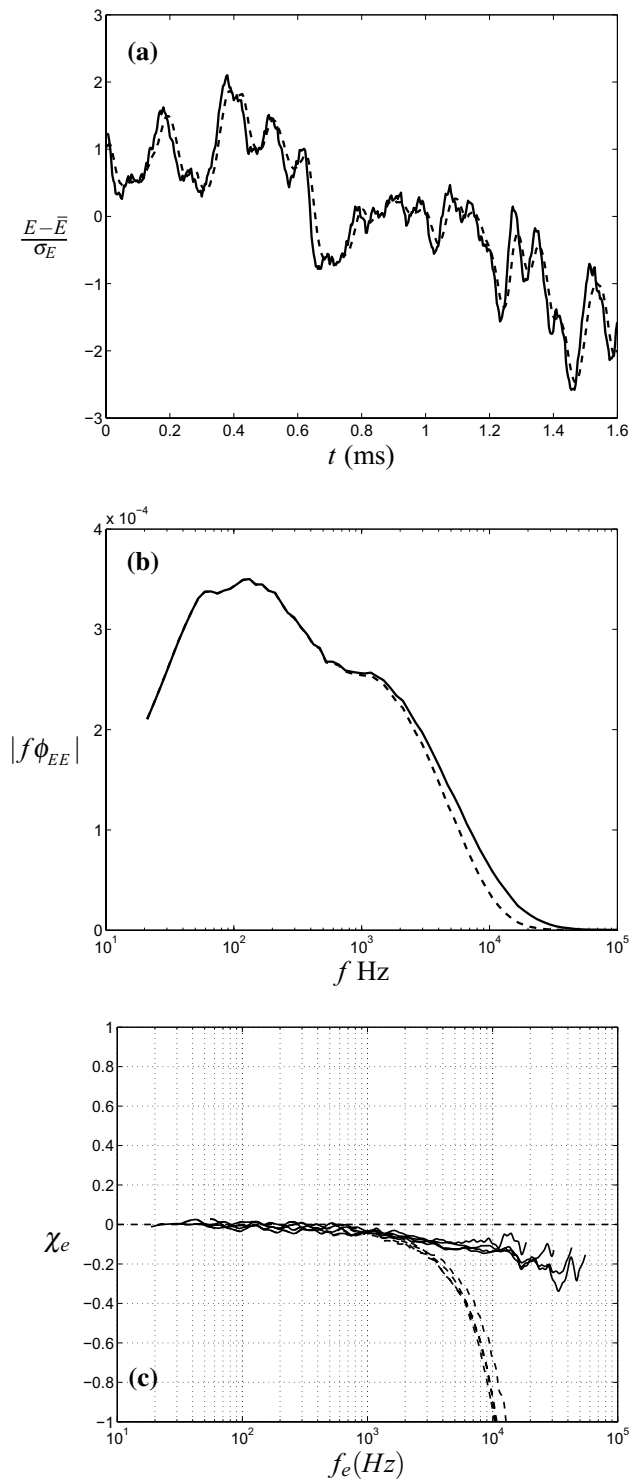

Fig. 7 Comparison of amplified and unamplified output from CTA3 at $z^+ = 80$. **a** Comparison of normalised raw fluctuating voltage signal, **b** comparison of normalised pre-multiplied energy spectra of streamwise velocity fluctuations, **c** comparison of the transfer function χ_e. In all plots, *solid lines* are the unamplified output and *dashed lines* are the amplified

Table 4 Experimental parameters for the five matched cases for CTA2 and NSTAP probe for $z^+ \approx 29$ experiment

e	Pressure (kPa)	$\nu\ (\times 10^6)\ (m^2\,s^{-1})$	$U_0\ (ms^{-1})$	$U_\tau\ (ms^{-1})$	Re_τ	z (mm)	z^+	l (mm)	l^+	Probe	$f^+ = 0.01$ (kHz)
1	246	6.21	26.9	1.00	10,380	0.18	28.9	0.06	9.6	NSTAP	1.60
2	334	4.65	20.1	0.74	10,350	0.18	28.8	0.06	9.6	NSTAP	1.19
3	463	3.36	14.5	0.54	10,360	0.18	28.8	0.06	9.6	NSTAP	0.86
4	758	2.05	8.9	0.33	10,350	0.18	28.8	0.06	9.6	NSTAP	0.52
5	2,154	0.72	3.1	0.11	10,280	0.18	28.6	0.06	9.5	NSTAP	0.18

measured temporal response for CTA3 in the near-wall position. Figure 6b shows the tuned frequency response indicated by an electrical pulse test. In this case, CTA3 displays behaviour that is inconsistent with CTA1 and CTA. The electrical test response curve (Fig. 6b) suggests that the anemometer system is noticeably under-damped; however, the experimentally determined transfer function χ_e shown in plot (a) exhibits behaviour more typical of an over-damped system.

It should be noted that CTA3 has an internal impulse test (rather than the square-wave test used by CTA1 and CTA2). Freymuth (1967) and Weiss et al. (2001) suggest that the response of the bridge to a square-wave voltage input best indicates the system response to an impulse of velocity. For comparison, we can attempt to recover the square-wave response from the impulse test by integrating the impulse test response, the result of which is shown in grey on Fig. 6b. The electronic test results can be used to predict the cut-off frequency by measuring the time τ_c for the initial response to decay to 3 % of the maximum and using this result in Eq. (1). It should be noted here that Eq. (1) is strictly only valid for optimally tuned square-wave responses (which is not the case here). However, for the impulse test, the measured τ_c indicates a cut-off frequency $f_c \approx 100$ kHz. The integrated impulse would suggest that $f_c \approx 50$ kHz. These results are in contrast to the direct test shown in Fig. 6a which indicates a -3 dB cut-off (where $\chi_e < -0.5$) occurs at $f_c = 17$ kHz. Hence, neither electronic test accurately conveys the measured -3 dB cut-off of the system to velocity fluctuations as determined by χ_e. The blue dot-dashed and red dashed curves on Fig. 6a shows the normalised energy spectrum of the impulse response and integrated impulse response respectively. Unlike the tests of CTA1 and CTA2, neither spectra seem to match the response indicated by χ_e. However, it is noted from Fig. 6a that the square-wave response gives a slightly better match to the experimentally determined performance (at least indicating an over-damped tendency). It is also worth noting that integration of the impulse is extremely sensitive to measurement accuracy.

In order to explore further the discrepancy shown in Fig. 6, the behaviour of the amplifier for CTA3 is investigated in Fig. 7a, which shows the fluctuating voltage signal sampled from both the amplified and unamplified anemometer outputs simultaneously. An analysis of the two signals indicates that the amplifier gain is approximately 15. For comparison on the same plot, both signals have been normalised by the standard deviation. The amplified signal is shown by the dashed line and the unamplified by the solid line. Figure 7a suggests that the amplified signal contains less high frequency information. This is confirmed in Fig. 7b which shows the normalised premultiplied energy spectra of voltage fluctuations (spectra are normalised in the same manner as discussed in Sect. 3.2). The filtering effect of the amplifier becomes noticeable at frequencies in excess of 1 kHz, beyond which the amplified spectra (dashed curve) exhibit increasingly attenuated energy as compared to the unamplified (solid line). It should be noted that these energy spectra are for experiment $e = 1$, the highest frequency case. Thus, there is already a certain degree of attenuation in these spectra owing to the temporal response of the system. Figure 7c shows the transfer function χ_e for both amplified and unamplified signals. Beyond $f_e \approx 2$ kHz, the degree of attenuation is increasingly worse for the amplified output. By $f_e = 10$ kHz, the amplified signal has an attenuation that is five times greater than the unamplified signal. In the limit of very high frequency and high gains, one would expect the amplifier to act as a filter. However, it is puzzling here that with only moderate gain the filtering becomes noticeable at such low frequencies. For typical instrument amplifiers with a gain-bandwidth product of say $O(10$ MHz$)$ and a gain of 15, one would not expect to attenuate signals until $f \gtrsim 500$ kHz.

4.4 NSTAP (with CTA2)

The final set of tests explores the temporal response of the Princeton NSTAP probe. This is a subminiature probe with a 100 nm $\times$ 2 μm $\times$ 60 μm platinum-sensing element, constructed using semiconductor and MEMS manufacturing techniques (for full details see Kunkel et al. 2006; Bailey et al. 2010; Vallikivi et al. 2011). Experimental conditions are given in Table 4. The important detail to notice here is that the sensor length l is almost an order of magnitude smaller than the standard probes used in preceding tests. Figure 8a shows the calculated transfer function χ_e for the NSTAP experiments.
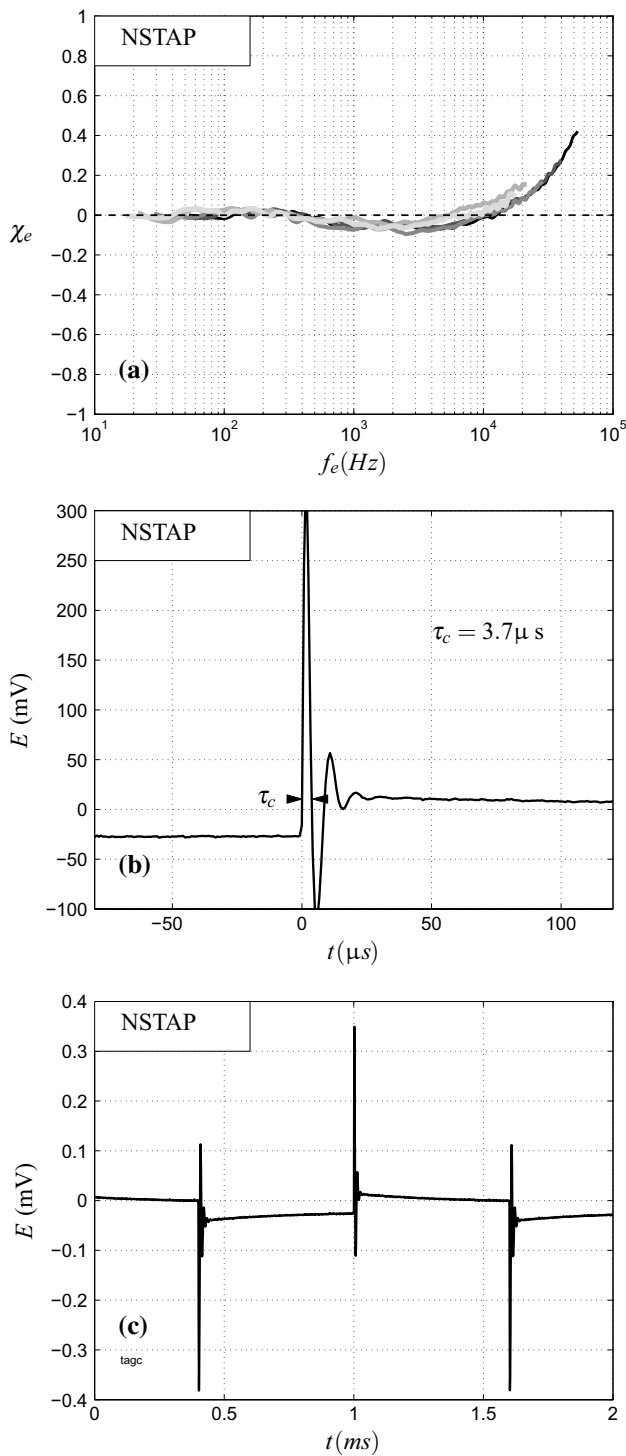
Fig. 9 Comparison of the transfer function χ_e for the same anemometer, but different probes (*grey*) standard probe at $z^+ \approx 80$ (*black*) NSTAP at $z^+ \approx 29$

Fig. 8 **a** The difference function χ_e for the NSTAP probe and CTA2 at $z^+ \approx 29$. *Line shading* indicates centreline velocity from *light* (lowest U_0, $e = 5$) to *dark* (highest U_0, $e = 1$). **b** Corresponding square-wave response, **c** expanded view of the square-wave response

The temporal response of the NSTAP/CTA2 system is much different and much improved, compared with the same system operating standard probes. There is still a region of
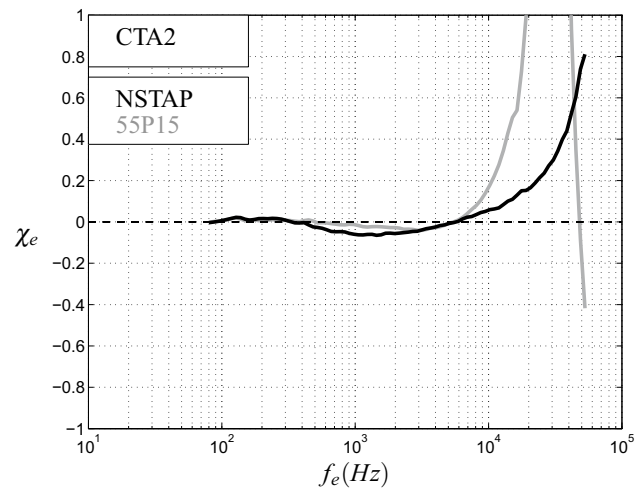
attenuation in the approximate range $500 < f_e < 5{,}000$ Hz. Beyond $f_e \approx 5$ kHz, there is a region of over-amplification. However, the increase of this amplification with increasing f_e is much more gradual than for other probe types. As a comparison, Fig. 9 plots the average χ_e (for $e = 1$–4) versus f_e for the standard probe (grey) and the NSTAP probe (black) both operating with CTA2. From this comparison, it is clear that the over-amplification occurring for $f_e > 5$ kHz is much more gradual and much less severe for the NSTAP probe. It should be noted that the standard probe was tested at $z^+ \approx 80$ and the NSTAP was tested at $z^+ \approx 29$, and also the square-wave response could not be tuned exactly the same, and so Fig. 9 is not quite a direct comparison of the two probe types. It is also noted that in neither case was the system optimally tuned, and thus, there is ambiguity regarding what would be the best possible response that could be obtained from each system. However, in general, Fig. 9 offers a clear indication of the extra temporal performance that can be gained with a given system by miniaturizing the sensor.

Figure 8b shows the sampled square-wave response test for the NSTAP experiment. Comparing this plot with Fig. 5 reveals that, for these under-damped cases, the NSTAP sensor yields a faster response. The timed decay of the initial step input $\tau_c = 3.7 \, \mu s$ for the NSTAP sensor. Based on this value, Eq. (1) suggests a -3 dB drop-off of 200 kHz. This is beyond the frequency at which we can accurately determine χ_e; however, Fig. 8a does suggest that $\chi_e < -0.5$ will occur well beyond 50 kHz (although it should be noted that there will be growing error due to under-damped resonant type behaviour for $f \gtrsim 20$ kHz). Unfortunately, it is not possible to plot the normalised energy spectrum of this square-wave response on Fig. 8a for comparison with the χ_e curve. The square-wave response measured for CTA2

with the NSTAP probe exhibits a very unusual higher-order response. This is clear by viewing a longer time history of the square-wave response as shown in Fig. 8c. The gradual decay occurring after each step input over a time-scale of approximately 0.5 ms gives a nonsensical Bode plot.

5 What does this mean to the accuracy of measurements in wall-bounded turbulence?

Figure 10a collates all experimentally determined transfer functions χ_e onto a single plot. Each coloured curve shows the average response[3] for a particular system and set of conditions as detailed in the key. If we combine these curves with a known energy spectrum from a wall-bounded turbulent flow, it is possible to make predictions of the overall attenuation due to frequency response. For this, we make use of the hot-wire measurements reported in Hutchins et al. (2009) for a flat-plate zero-pressure-gradient turbulent boundary layer at $Re_\tau \approx 7{,}300$. Since the freestream velocity for these measurements was only 10 ms^{-1}, we do not expect any major temporal resolution error for these original data. We will refer to these original results using subscript o. At each of 53 wall-normal measurement locations (logarithmically spaced from $8 < z^+ < 1.4Re_\tau$), we can produce an energy spectrum ϕ_{uu} as a function of frequency f_o for these original data. A new boundary layer (denoted with subscript n) with the same Reynolds number but an increased freestream velocity U_∞ will have turbulent energy shifted to higher frequencies in Hz (see Fig. 3 for example). Yet, assuming Reynolds number similarity, the original and the new pre-multiplied energy spectra will collapse when scaled with viscous variables (f^+ vs $k_x\phi_{uu}^+$). More precisely, since the ratio $|u_\tau^2/\nu|_o$ for the original experiment is known, it is possible to predict the frequency content of the spectrum at some 'new' value of this ratio $|u_\tau^2/\nu|_n$ using,

$$f_n = f_o \left| \frac{\nu}{u_\tau^2} \right|_o \left| \frac{u_\tau^2}{\nu} \right|_n \tag{7}$$

These predicted unattenuated energy spectra at $z^+ = 15$ are shown by the black curves in Fig. 10b–d for $U_\tau^2/\nu \times 10^{-5}$ ratios of 0.305, 1.905 and 6.172 s^{-1}, respectively. For unpressurised facilities where the working fluid is air (assuming $\nu \approx 1.5 \times 10^{-5}$ m^2 s^{-1}), these ratios correspond to freestream velocities of approximately 20, 50 and 90 ms^{-1}. We will denote this unpressurised equivalent freestream velocity as $U_{\infty_{sa}}$. Combining these energy spectra with the transfer functions shown in Fig. 10a enables us

to predict the spectra (ϕ_{uu_p}) that would actually be measured by each of the anemometer configurations.

$$\phi_{uu_p}(f_n) = \phi_{uu_n}(f_n)\left[1 + \chi_e(f_n)\right] \tag{8}$$

It should be emphasised that these predicted spectra are valid only for the particular anemometer set-up employed here. A different user with different settings would obtain a different performance. Nonetheless, this analysis can serve as a useful indication of the likely errors due to heavily over- or under-damped systems. For Fig. 10b, which shows a case where $U_{\infty_{sa}} \approx 20$ ms^{-1}, the error for each of the anemometer configurations is minimal. At these conditions, the majority of turbulent energy is contained within a frequency range where plot (a) indicates the transfer functions are relatively flat, and hence, there is little sign of attenuation due to frequency response. However, as the ratio U_τ^2/ν increases, the turbulent energy is increasingly shifted to the right of plots (c) and (d) into a frequency range where the anemometer configurations studied here will attenuate or over-represent energy. For plot (c) where $U_\tau^2/\nu = 1.905 \times 10^5$ s^{-1}, corresponding to an unpressurised freestream velocity of approximately 50 ms^{-1}, we can begin to see differences developing in the spectra measured by each of the HWA configurations. In this case, these differences are most pronounced for the over-damped systems. For plot (d), where $U_\tau^2/\nu = 6.172 \times 10^5$ s^{-1}, corresponding to an unpressurised freestream velocity of approximately 90 ms^{-1}, the effect of frequency response is becoming acute for almost all systems tested (other than the NSTAP/CTA2 combination). Note that for these conditions, the heavily under-damped system (the standard 55P15 probe and CTA2) gives the largest error in spectra for all systems (giving a bigger error than CTA3 and over-damped CTA1). This is caused by the under-damped response and large resonant peak in the transfer function centred at $f \approx 31$ kHz. For this U_τ^2/ν ratio, substantial turbulent energy is located in this problematic frequency range leading to the large errors evident in Fig. 10d, e, h.

Figure 10e shows the percentage error in variance at $z^+ = 15$ corresponding to these predicted spectra as a function of U_τ^2/ν (lower abscissa) and unpressurised U_∞ (upper abscissa),
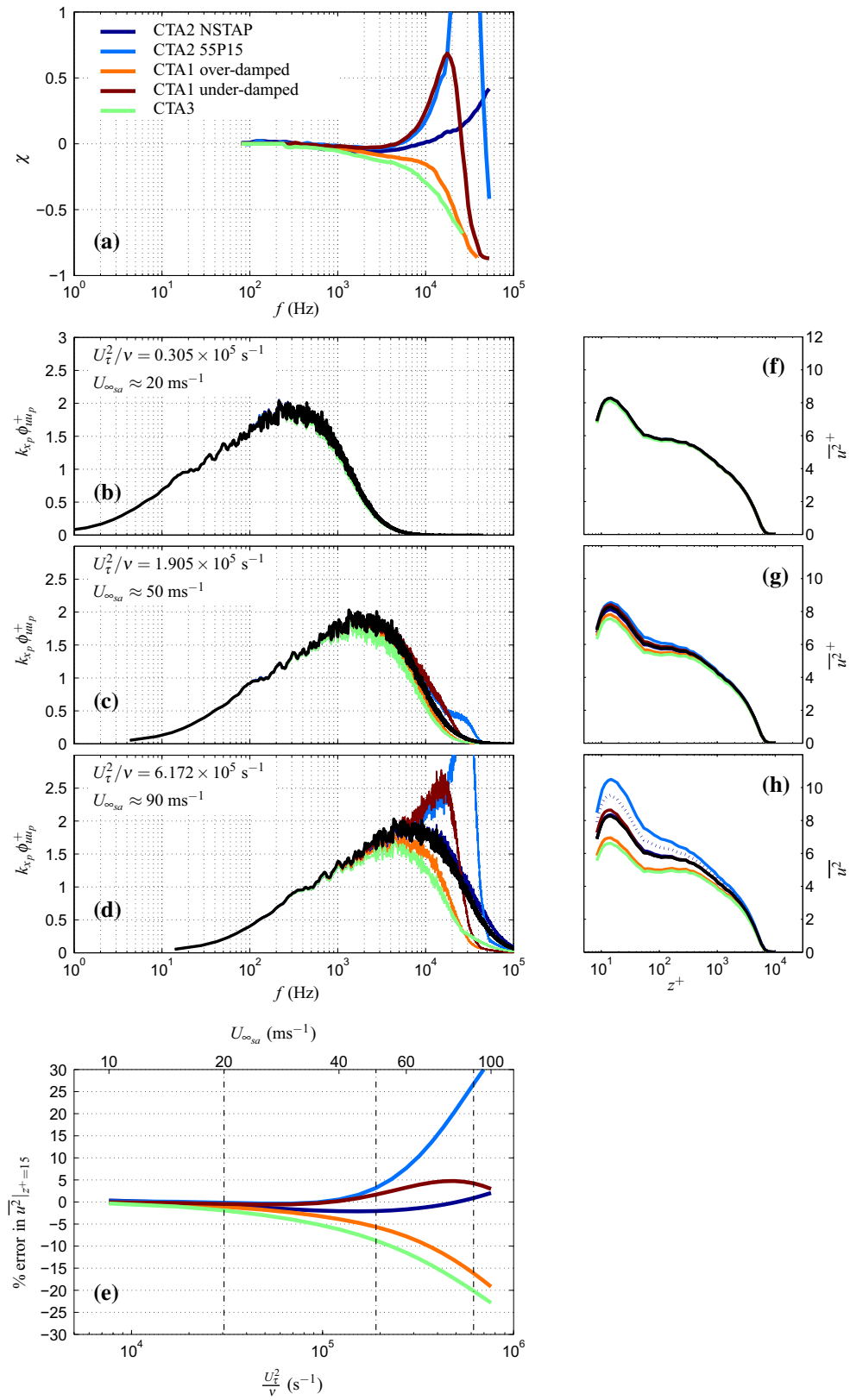
$$\% \text{ error in } \overline{u^2} = 100 \times \frac{(\overline{u^2})_p - (\overline{u^2})_n}{(\overline{u^2})_n}$$

where

$$(\overline{u^2})_p = \int (1 + \chi_e)\phi_{uu_n} dk_{x_n}, \quad (\overline{u^2})_n = \int \phi_{uu_n} dk_{x_n}$$

This could be a useful plot for experimentalists wishing to consider likely errors in experiments due to the frequency response of anemometer/probe system. Note that

---

[3] These average response curves are the mean of the χ_e verses f_e profiles determined for experiments $e = 1 \rightarrow 4$.

◀ **Fig. 10** Summary figure showing example expected errors owing to temporal response for the various tested HWA configurations. **a** *Compilation plot* showing the transfer functions for the tested systems, **b–d** the predicted measured energy spectra at $z^+ = 15$ and $Re_\tau \approx 7{,}000$ for three different $U_\tau^2/\nu \times 10^{-5}$ ratios of **a** 0.305 , **b** 1.905 and **c** 6.172 s^{-1}, corresponding to freestream velocities in unpressurised facilities of 20, 50 and 90 ms^{-1}, respectively. *Black curves* show correct result, and *coloured lines* show the predicted measurement based on the transfer function χ for each anemometer. **e** Percentage error in the variance at $z^+ = 15$, as a function of U_τ^2/ν (and $U_{\infty_{sa}}$) resulting from the temporal response of each HWA configuration. Plots **f–h** show the wall-normal profiles of variance for each HWA configuration for the three $U_\tau^2/\nu \times 10^5$ ratios. The *dashed line* in **h** shows predicted behaviour of the CTA2/NSTAP system at $U_\tau^2/\nu \approx 35 \times 10^5$ s^{-1}

for $U_\tau^2/\nu \lesssim 0.3 \times 10^5$ s^{-1} ($U_{\infty_{sa}} \lesssim 20\,\text{ms}^{-1}$) the errors in variance at $z^+ = 15$ are minimal for all systems. However, as U_τ^2/ν increases, the errors become more severe. For an unpressurised freestream velocity of 90 ms^{-1} in air, we would expect ~20 % attenuation of the variance measured by the over-damped systems, switching to a 25 % over-representation for the highly under-damped system (CTA2 with standard probe). It should be noted that although plot (e) indicates that the error in variance for the under-damped CTA1 appears to be small at $U_{\infty_{sa}} = 90\,\text{ms}^{-1}$, this should really just be considered an anomaly. The spectra in plot (d) are greatly distorted, but in a manner in which the attenuation approximately counteracts the over-representation. The time signal measured by this system would have significant errors for this U_τ^2/ν ratio.

Figure 10f–h extends the view from the near-wall, to consider the error due to frequency response across the entire layer. As U_τ^2/ν increases, the anemometer systems give increasingly inaccurate representations of the mean variance profile. The exception here is the NSTAP/CTA2 combination which works remarkable accurately up to $U_\tau^2/\nu = 6.172 \times 10^5$ s^{-1}. Even so, it should be noted that this system is not immune to errors. The NSTAP has been designed for use in the Princeton Superpipe, a pressurised facility. At very high Reynolds numbers, it is still conceivable that the ratio U_τ^2/ν will become large. For example, at a Reynolds number of $Re_\tau = 734{,}000$ as reported by Zagarola (1996), the ratio $U_\tau^2/\nu \approx 35 \times 10^5$ s^{-1}. The dotted line in Fig. 10h shows the predicted profile for the CTA2/ NSTAP configuration at this ratio. In considering this result, it should be noted that to-date the NSTAP has not been operated above $Re_\tau \approx 100{,}000$ due to limitations in structural strength.

There are several approximations involved in the creation of Fig. 10. The data of Hutchins et al. (2009) contain an inherent attenuation owing to the finite size of the sensing element ($l^+ = 22$). Also, the analysis is strictly only valid at the Reynolds number of the original data ($Re_\tau = 7{,}300$). As Reynolds number increases, an increasing proportion of

the broadband energy is due to large outer-scaled turbulent events. This would lead to slight reductions in the percentage errors presented in Fig. 10e. Such effects are a weak (logarithmic) function of Reynolds number (see Hutchins et al. 2009). In creating plots (b–h), the same transfer function χ is assumed for all wall-normal locations. In reality, χ will be a function of the local mean velocity and hence wall-normal location (z), with behaviour becoming increasingly damped close to the wall (refer to Appendix 1). In spite of these limitations, this analysis can provide a useful estimate of the errors arising from frequency response for HWA measurements in high Reynolds number wall-bounded turbulence. In general, HWA users should be cautious of flows that have substantial turbulent energy above the flat region of the response curves shown in Fig. 10a.

6 Conclusions

A novel direct method for testing the frequency response of hot-wire anemometers to velocity fluctuations has been proposed and tested. This method is shown to provide a consistent and reliable estimate of the transfer function arising from the temporal response of the anemometry system. Several HWA systems with differing configurations have been tested, and the implications of the determined frequency response to the accuracy of measurements in wall-bounded turbulence are considered. Based on these findings, we can draw the following conclusions and recommendations,

1. In flows where there is significant energy content beyond 5–7 kHz, the frequency response of HWA systems can potentially cause large measurement errors in turbulence quantities.
2. For wall-bounded turbulence, a convenient parameter to judge frequency content is the ratio U_τ^2/ν. The higher this ratio, the higher the frequency content of the turbulent energy.

   - For $U_\tau^2/\nu \lesssim 0.3 \times 10^5$ s^{-1}, error due to frequency response will be minimal. This seems to be true for the three systems tested, regardless of whether the system is over- or under-damped.
   - For $U_\tau^2/\nu \gtrsim 2 \times 10^5$ s^{-1}, errors due to frequency response become significant (for $U_\tau^2/\nu \approx 6 \times 10^5$ s^{-1}, misrepresentation of energy can exceed ±20 % for heavily over- and under-damped systems respectively).

3. For CTA1 and CTA2, the energy spectrum of the square-wave response gives a reasonably good indication of the true response of the system, at least indicating over- or under-damped behaviour and showing the

location of any resonant peaks. The exception to this is CTA3, which has an electrical response that seems at odds with the measured response of the system. This variability unfortunately suggests that the high-frequency performance of each anemometer must be carefully and directly ascertained (through non-electronic means, such as the method detailed here) prior to reliable high-frequency measurements.

4. The standard -3 dB drop-off can be misleading. Caution should be exercised when interpreting the square-wave response. The standard -3 dB drop-off (as estimated using Eq. 1) is an overly liberal estimate of the upper limiting frequency f_c for accurate boundary layer measurements (since -3 dB represents a 50 % attenuation in measured energy). For under-damped systems, there is a substantial error due to over-representation of the turbulent energy at frequencies approximately a decade lower than f_c determined in this manner (under-damped systems will exhibit attenuation in this frequency range).

5. The response should be carefully checked across the expected range of operating conditions. For systems with behaviour similar to CTA1 and CTA2, viewing the energy spectrum of the square-wave response in real time while tuning the response of the anemometer might be the most promising method for attaining a flat response. Figure 3 demonstrates that changes in the square-wave response that can outwardly appear quite minor can indicate a profound shift from over- to under-damped behaviour. Consequently, HWA systems that are 'optimally' tuned in the freestream, might be over-damped close to the surface of a wall-bounded turbulent flow (see Appendix 2).
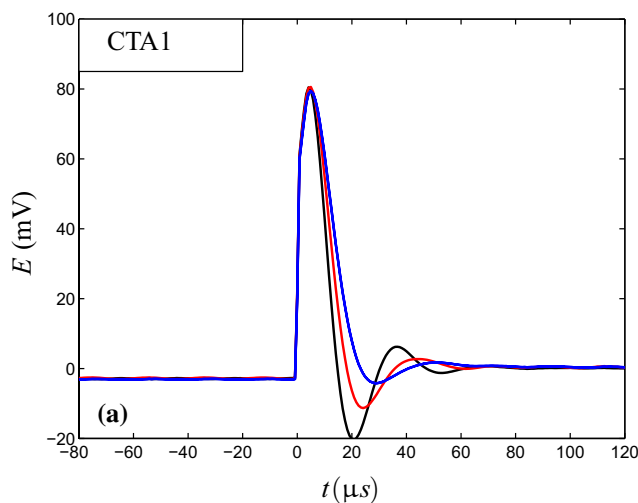
6. Smaller sensing elements help. Preliminary measurements indicate that, when operated in an under-damped configuration, CTA2 with the NSTAP probe has an improved frequency response as compared to the same under-damped system with a standard probe geometry. Though these two experiments cannot be considered directly comparable, the results suggest that miniaturized sensors could hold a great promise for improved HWA measurements in high-frequency flows.

Appendix 1: Variation of response within a boundary layer

Figure 11a shows the square-wave response measured in the freestream of a boundary layer wind tunnel (the Melbourne HRNBLWT) at various mean velocities $\overline{U} = 10$, 3 and 1 ms^{-1} (black, red and blue curves, respectively). The HWA system consists of CTA1 and a standard 55P15 probe. The anemometer has not been adjusted between these experiments, and thus, any difference between the three curves in Fig. 11 is purely a result of the altered mean velocity. Figure 11b shows the corresponding normalised energy spectrum of the square-wave response, which for CTA1 is shown to give a reasonable representation of the *directly* determined response χ (see Fig. 3).
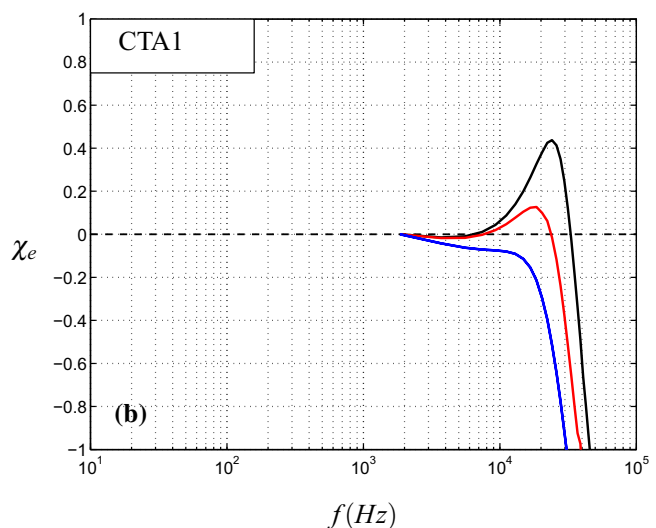

Fig. 11 Change with local mean velocity of **a** the square-wave response and **b** the normalised energy spectrum of the square-wave response. *Black* $\overline{U} = 10.7$ ms^{-1}, *red* $\overline{U} = 3.5$ ms^{-1}, *blue* $\overline{U} = 1.0$ ms^{-1}. Tuning of anemometer has not been altered (changes are due only to the change in $\overline{U}$)

The variation in mean velocity over the sensor causes a pronounced change in the measured response, shifting from an under-damped system at $10\,\mathrm{ms}^{-1}$ to a clear over-damped behaviour at $1\,\mathrm{ms}^{-1}$. Such behaviour is to be expected from the heat transfer equation. As $\overline{U}$ reduces from 10 to $1\,\mathrm{ms}^{-1}$, the wire Reynolds number has been decreased by a factor of approximately 10 reducing the heat transfer or cooling from the wire by a factor of approximately 3. Reduced heat transfer leads to increased damping. This is evident in Fig. 11 with the system switching from under- to over-damped behaviour as the mean velocity reduces.

Figure 11 suggests that it is essential to check the square-wave response across the entire expected velocity range prior to a boundary layer traverse experiment. If the frequency response is only checked at freestream conditions (say $10\,\mathrm{ms}^{-1}$), a system could encounter substantial temporal resolution issues close to the wall as the system becomes increasingly damped. For a wall-bounded turbulent flow with a freestream velocity of $10\,\mathrm{ms}^{-1}$, local mean velocities of 3 and $1\,\mathrm{ms}^{-1}$ would be encountered at $z^{+} \approx 10$ and 3. Hence, the temporal response of the system would shift from under-damped to over-damped as the probe was traversed very close to the surface.

Appendix 2: Determining the square-wave response

The square-wave responses shown throughout this investigation were obtained with the probe at the pipe centreline, with the centreline velocity and pressurisation matched to the local conditions at the probe location (which was either $z^{+} = 29$ or 80) for the baseline experiment $e5$. Since the pipe core is fully turbulent, the injected square-wave response is superimposed over a turbulent signal. For analysis, the signal is sampled at 1.2 MHz for a duration of 10 s. An example of this sampled signal for the under-damped CTA1 (as detailed in Figs. 1, 2, 3) is shown in Fig. 12a, with an inset showing an enhanced detail of the square-wave response superimposed onto the turbulent core flow. To separate the square-wave response from the turbulent signal, the sampled data are filtered using a sharp spectral high-pass filter at $f = 7$ kHz. An example of the resulting filtered signal is shown in Fig. 12b. Note that the cut-off filter was selected to remove the large-scale turbulent component from the signal. A simple threshold technique is used to extract the square-wave response. In the case shown, a threshold of 0.04 V was used detect the rising edge of the square-wave input. Regions where the rising part of the signal exceeded this threshold are shown by the dot symbols on Fig. 12b. A region of the signal surrounding this threshold crossing is then extracted and added to an ensemble average as shown in Fig. 12c. The
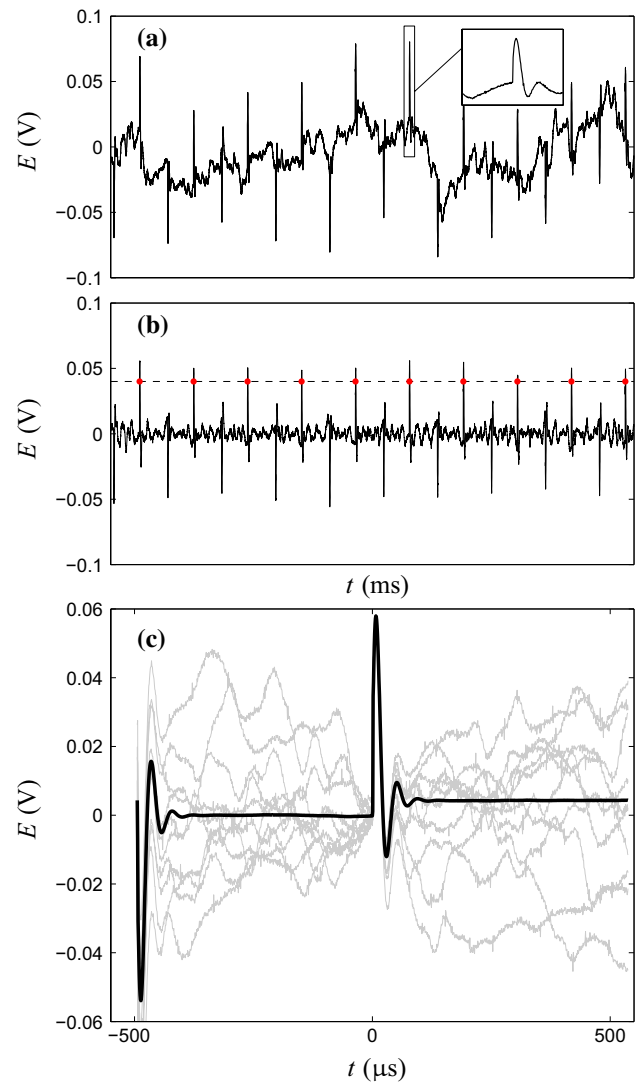

Fig. 12 Plots illustrating the extraction of the square-wave response from a turbulent signal measured in the core. **a** Original time series of the velocity output from the anemometer (sampled at 1.2 MHz) showing square-wave response superimposed onto turbulent signal, inset shows an expanded detail of the response to rising step function. **b** Data high-pass filtered at 7 kHz, *dashed line* shows detection threshold and *red dots* show rising edge detection. **c** Ensemble average of detected rising edge step responses, *grey lines* shows the individual detections shown in plots **a** and **b** and *black curve* shows ensemble average over 10 s of data (approximately 10,000 individual occurrences)

grey curves show the square-wave responses extracted from Fig. 12b. The black curve shows the average response.

References

Ashok A, Bailey S, Hultmark M, Smits A (2012) Hot-wire spatial resolution effects in measurements of grid-generated turbulence. Exp Fluids 53(6):1713–1722. doi:10.1007/s00348-012-1382-5

Bailey SC, Kunkel GJ, Hultmark M, Vallikivi M, Hill JP, Meyer KA, Tsay C, Arnold CB, Smits AJ (2010) Turbulence measurements using a nanoscale thermal anemometry probe. J Fluid Mech 663:160–179

Bonnet JP, de Roquefort TA (1980) Determination and optimization of frequency response of constant temperature hot-wire anemometers in supersonic flows. Rev Sci Instrum 51:234–239

Bruun HH (1995) Hot-wire anemometry. Oxford University Press, Oxford

Chin CC, Hutchins N, Ooi ASH, Marusic I (2009) Use of direct numerical simulation (DNS) data to investigate spatial resolution issues in measurements of wall-bounded turbulence. Meas Sci Technol 20(11):115,401

Chin CC, Hutchins N, Ooi A, Marusic I (2011) Spatial resolution correction for hot-wire anemometry in wall turbulence. Exp Fluids 50:1443–1453

Comte-Bellot G (1976) Hot-wire anemometry. Annu Rev Fluid Mech 8:209–231

Fernholz HH, Krausse E, Nockermann M, Schober M (1995) Comparative measurements in the canonical boundary layer at $Re_{\delta_2} \leqslant 6 \times 10^4$ on the wall of the German–Dutch windtunnel. Phys Fluids 7(6):127

Freymuth P (1967) Feedback control theory for constant-temperature hot-wire anemometers. Rev Sci Instrum 38(5):677–681

Freymuth P (1977) Frequency response and electronic testing for constant-temperature hot-wire anemometers. J Phys E Sci Instrum 10(7):705–710

Hites MH (1997) Scaling of high-Reynolds number turbulent boundary layers in the National Diagnostic Facility. PhD thesis, Illinois Institute of Technology, Chicago

Hutchins N, Nickels TB, Marusic I, Chong MS (2009) Hot-wire spatial resolution issues in wall-bounded turbulence. J Fluid Mech 635:103–136

Khoo BC, Chew YT, Li GL (1995) A new method by which to determine the dynamic response of marginally elevated hot-wire anemometer probes for near-wall velocity and shear stress measurements. Meas Sci Technol 6:1399–1406

Kidron I (1966) Measurement of the transfer function of hot-wire and hot-film turbulence transducers. IEEE Trans Instrum Meas 15:76–81

Ko NWM, Ho KK (1977) On the determination of frequency response of hot-wire system. IEEE Trans Instrum Meas 26(4):360–367

Kunkel GJ, Arnold CB, Smits AJ (2006) Development of NSTAP: nanoscale thermal anemometry probe. AIAA-paper 2006-3718

Li JD, Mckeon BJ, Jiang W, Morrison JF, Smits AJ (2004) The response of hot wires in high Reynolds-number turbulent pipe flow. Meas Sci Technol 15:789–798

Ligrani PM, Bradshaw P (1987) Spatial resolution and measurement of turbulence in the viscous sublayer using subminiature hot-wire probes. Exp Fluids 5:407–417

Monkewitz PA, Duncan RD, Nagib HM (2010) Correcting hot-wire measurements of stream-wise turbulence intensity in boundary layers. Phys Fluids 22(091):701

Morrison JF, McKeon BJ, Jiang W, Smits AJ (2004) Scaling of the streamwise velocity component in turbulent pipe flow. J Fluid Mech 508:99–131

Nickels TB, Marusic I, Hafez S, Hutchins N, Chong MS (2007) Some predictions of the attached eddy model for a high Reynolds number boundary layer. Philos Trans R Soc A 365:807–822

Örlü R, Alfredsson PH (2010) On spatial resolution issues related to time-averaged quantities using hot-wire anemometry. Exp Fluids 49:101–110

Österlund JM (1999) Experimental studies of zero pressure-gradient turbulent boundary-layer flow. PhD thesis, Department of Mechanics, Royal Institute of Technology, Stockholm

Oxlade AR, Valente PC, Ganapathisubramani B, Morrison JF (2012) Denoising of time-resolved piv for accurate measurement of turbulence spectra and reduced error in derivatives. Exp Fluids 53:1561–1575

Perry AE, Li JD (1990) Experimental support for the attached-eddy hypothesis in zero-pressure-gradient turbulent boundary layers. J Fluid Mech 218:405–438

Perry AE, Morrison GL (1970) Static and dynamic calibrations of constant temperature hot-wire systems. J Fluid Mech 47:765–777

Segalini A, Cimarelli A, Rüedi JD, Angelis ED, Talamelli A (2011a) Effect of the spatial filtering and alignment error of hot-wire probes in a wall-bounded turbulent flow. Meas Sci Technol 22(10):105,408

Segalini A, Örlü R, Schlatter P, Alfredsson PH, Rüedi JD, Talamelli A (2011b) A method to estimate turbulence intensity and transverse Taylor microscale in turbulent flows from spatially averaged hot-wire data. Exp Fluids 51:693–700

Smits AJ, Zagarola MV (2005) Applications of dense gases to model testing for aeronautical and hydrodynamic applications. Meas Sci Technol 16:1710–1715

Smits AJ, Monty JP, Hultmark M, Bailey SC, Hutchins N, Marusic I (2011) Spatial resolution correction for wall-bounded turbulence measurements. J Fluid Mech 676:41–53

Talamelli A, Persiani F, Fransson JHM, Alfredsson PH, Johansson AV, Nagib HM, Rüedi JD, Sreenivasan KR, Monkewitz PA (2009) CICLoPE—a response to the need for high reynolds number experiments. Fluid Dyn Res 41(2):021407. doi:10.1017/S0022112089002892

Valente PC, Vassilicos JC (2011) Comment on "Dissipation and decay of fractal-generated turbulence". Phys Fluids 23(119):101

Vallikivi M, Hultmark M, Bailey S, Smits A (2011) Turbulence measurements in pipe flow using a nano-scale thermal anemometry probe. Exp Fluids 51(6):1521–1527

Watmuff JH (1995) An investigation of the constant-temperature hot-wire anemometer. Exp Therm Fluid Sci 11(2):117–134

Weiss J, Knauss H, Wagner S (2001) Method for the determination of frequency response and signal to noise ratio for constant-temperature hot-wire anemometers. Rev Sci Instrum 72(3):1904–1909

Zagarola MV (1996) Mean flow scaling of turbulent pipe flow. PhD thesis, Department of Mechanical and Aerospace Engineering, Princeton University, USA

Zagarola MV, Smits AJ (1998) Mean-flow scaling of turbulent pipe flow. J Fluid Mech 373:33–79